Regenerative Therapy 24 (2023) 515–527

Contents lists available at ScienceDirect

Regenerative Therapy

journal homepage: http://www.elsevier.com/locate/reth

Original Article

Collagen type I-based recombinant peptide promotes bone regeneration in rat critical-size calvarial defects by enhancing osteoclast activity at late stages of healing

Ichinnorov Chimedtseren [a, b], Shoji Yamahara [b, c], Yasunori Akiyama [a, b], Masaaki Ito [a, b], Yoshinori Arai [e], Anar Erdene Gantugs [a], Nagato Nastume [a], Taku Wakita [d], Takahiro Hiratsuka [d], Masaki Honda [b], Jorge Luis Montenegro Raudales [b, *]

[a] Division of Research and Treatment for Oral and Maxillofacial Congenital Anomalies, School of Dentistry, Aichi Gakuin University, 2-11 Suemori-dori, Chikusa-ku, Nagoya, Aichi, 464-8651, Japan
[b] Department of Oral Anatomy, School of Dentistry, Aichi Gakuin University, 1-100 Kusumoto-cho, Chikusa-ku, Nagoya, Aichi 464-8650, Japan
[c] Department of Orthodontics, School of Dentistry, Aichi Gakuin University, 2-11 Suemori-dori, Chikusa-ku, Nagoya, Aichi, 464-8651, Japan
[d] Bio Science & Engineering Laboratory, FUJIFILM Corporation, 577 Ushijima, Kaisei-machi, Ashigarakami-gun, Kanagawa 258-8577, Japan
[e] Department of Oral and Maxillofacial Radiology, Nihon University School of Dentistry, 1-8-13 Kanda-Surugadai, Chiyoda-ku, Tokyo 101-8310, Japan

ARTICLE INFO

Article history:
Received 27 July 2023
Received in revised form
10 September 2023
Accepted 21 September 2023

Keywords:
Bone regeneration
Bone graft material
Calvaria
Recombinant human collagen peptide
Osteoblast
Osteoclast

ABSTRACT

Introduction: We recently demonstrated the bone-forming potential of medium-cross-linked recombinant collagen peptide (mRCP) in animal models of bone defects. However, these studies were limited to a 4-week observation period; therefore, in the present study, we aimed to further evaluate mRCP as a suitable bone graft material for the alveolar cleft by analyzing its bone-forming potential, osteogenic-inducing ability, and biodegradation over an extended period of 12 weeks, using a rat critical-size calvarial defect model.

Methods: Using Sprague-Dawley rats, we created critical-size calvarial defects through a surgical procedure. The defects were then filled with 3 mg of mRCP (mRCP group) or 18 mg of Cytrans® (CA) granules, which has a carbonate apatite-based composition resembling natural bone, was used as a reference material (CA group). For negative control, the defects were left untreated. Bone volume, total bone volume (bone volume including CA granules), and bone mineral density (BMD) in the defect were assessed using micro-computed tomography (μ-CT) at 0, 4, 8, and 12 weeks after implantation. Using histomorphometric analyses of hematoxylin and eosin (H&E)-stained sections, we measured the amount of newly formed bone and total newly formed bone (new bone including CA granules) in the entire defect site, as well as the amount of newly formed bone in the central side, two peripheral sides (left and right), periosteal (top) side, and dura mater (bottom) side. In addition, we measured the amount of residual bone graft material in the defect. Osteoclasts and osteoblasts in the newly formed bone were detected using tartrate-resistant acid phosphatase (TRAP) and alkaline phosphatase (ALP) staining, respectively.

Results: Bone volume in the mRCP group increased over time and was significantly larger at 8 and 12 weeks after surgery than at 4 weeks. The bone volume in the mRCP group was greater than that of the CA and control groups at 4, 8, and 12 weeks after implantation, and while the total bone volume was greater in the CA group after 4 and 8 weeks, the mRCP group had comparable levels of total bone volume to that of the CA group at 12 weeks after implantation. The BMD of the mRCP group reached similar levels to native calvaria bone at the same time point. H&E-stained sections revealed a larger amount of newly formed bone 12 weeks after implantation in the mRCP group compared to that of the CA and control groups. The total newly formed bone at 12 weeks after implantation was on par with that in the CA group. Furthermore, at the defect site, the area of newly formed bone was larger on the peripheral and dura mater sides. Notably, the number of osteoclasts in the mRCP group was higher than in the CA and

Abbreviations: RCP, recombinant collagen peptide; mRCP, medium-cross-linked RCP; RGD, arginyl-glycyl-aspartic acid; μ-CT, micro-computed tomography; BMD, bone mineral density; ROIs, regions of interest; H&E, hematoxylin and eosin; ALP, alkaline phosphatase; TRAP, tartrate-resistant acid phosphatase; SD, standard deviation.

* Corresponding author.
E-mail address: jlmonrau@dpc.agu.ac.jp (J.L. Montenegro Raudales).

Peer review under responsibility of the Japanese Society for Regenerative Medicine.

https://doi.org/10.1016/j.reth.2023.09.013

control groups and peaked 8 weeks after implantation, which coincided with the timing of the greatest resorption of mRCP. Although the ALP-positive area was greater in the mRCP group compared to other groups, we did not detect any significant changes in the number of osteoblasts over time.
Conclusion: This study demonstrated the bone-forming potential of mRCP over an extended period of 12 weeks, suggesting that mRCP sufficiently resists resorption to promote bone formation through induction of osteoclast activation in the late stages of the healing period.

1. Introduction

Alveolar cleft is a skeletal defect resulting from disturbances during the development of the primary palate. Justification for alveolar cleft repair is based not only on aesthetic value, but also on achieving maxillary arch stabilization, tooth eruption, closure of the nasolabial fistula, and speech improvement [1,2]. Bone grafting is the most common method for alveolar cleft repair, and autologous bone from the iliac crest is the preferred bone graft material because it is osteoinductive, osteoconductive, and biomechanically stable, serves as a niche for incoming cells and blood vessels, and provides growth factors for the differentiation of stem cells to osteogenic cells [3]. Yet, the invasiveness of the harvesting procedure and operative complications such as donor site morbidity, including possible scarring, pain, and cutaneous nerve injury, have prompted researchers to design new artificial bone substitutes [4–6]. However, incorporating all the favorable attributes of autologous bone into the design of a bone graft material represents a major challenge in tissue engineering.

Therefore, researchers have focused their efforts on developing bone graft materials based on the major components of the body, such as collagen-based materials. Collagen is one of the most abundant proteins in the organism, and type I collagen is the main protein in the extracellular matrix (ECM) of bones [7]. Collagen-based materials have shown merits in regenerative medicine, as demonstrated by their osteoconductive and osteoinductive properties, low antigenicity, biodegradability, and ability to promote cell adhesion, proliferation, and differentiation [8,9]. Nevertheless, the animal-derived origins of these materials cast doubt on their safety owing to potential disease transmission [10].

To overcome these issues, researchers have developed a collagen type I-based recombinant protein (RCP), commercially available as Cellnest® (FUJIFILM), derived from the *Pichia pastoris* yeast. This innovative design is based on the human alpha-1 sequence (α 1 chain) and possesses 12 arginyl-glycyl-aspartic acid (RGD) motifs in a single molecule, allowing for improved osteoinduction, angiogenesis, and biodegradation [11–14], thus satisfying the requirements of an ideal bone graft without the risk of disease transmission [15]. Several animal studies have described the fundamental characteristics of RCP as a promising graft material, demonstrating its efficiency as a platform for cellular implantation, angiogenic stimulation, cell recruitment, and bone formation [14,16,17].

We have previously performed a series of preclinical studies to gain insights into the characteristics of RCP and its suitability as a bone graft material for alveolar clefts. We first demonstrated an enhanced bone-regenerative effect when using block-shaped RCP as a scaffold in combination with lipid-free dedifferentiated cells in rat critical-size mandibular defects [18]. Considering that the cross-linking of collagen-based materials affects their structural and mechanical properties [19] (i.e., biodegradation rate and water absorption), we evaluated the appropriate cross-linking density for the bone-forming potential of RCP as a standalone graft material in particle form. Among low, medium, and high cross-linking, medium cross-linked (mRCP) presented the greatest bone-forming potential in a rat palatine fissure model [11].

Therefore, we then used mRCP in a rat critical-size calvarial defect to compare its performance against autologous bone from the rat tibia and showed that mRCP induced comparable levels of bone formation to autologous bone [20]. Our latest report showed the effects of different pore sizes on the bone-forming potential of mRCP. Because pore size affects cellular activities such as cell penetration, migration, survival, and differentiation [21], to further optimize the use of mRCP as a bone graft material, we analyzed the effect of different interconnected pore sizes of mRCP in a rat critical-size calvarial defect model. The results showed that the optimal pore size of mRCP for inducing bone formation ranged between 100 and 300 μm [22]. Taken together, these studies not only show the bone-regenerative potential of mRCP, but also its versatility to fit the needs of the desired application.

The above-mentioned reports all showed a positive effect of mRCP on bone regeneration, as evidenced by the histological findings of newly formed bone and verified by the presence of osteoblasts and osteoclasts, which are critical for bone remodeling [23]. However, these studies were conducted over a 4-week period. A bone graft material should provide sufficient mechanical support until new bone formation occurs [24]. In particular, for alveolar cleft repairs that require subsequent orthodontic treatment, orthodontic movement is initiated at an average of three months after bone grafting [25,26]. Moreover, we are yet to assess the osteogenic inducing ability of mRCP over a longer period. Hence, questions remain regarding the validity of mRCP as a bone graft material for the alveolar cleft. Therefore, in the present study, we aimed to examine the bone-forming potential, osteogenic inducing ability, and biodegradation of mRCP over an extended period of 12 weeks to further evaluate mRCP as a bone graft material using a rat critical-size calvarial defect model. Additionally, we compared its performance with that of the commercially available bone substitute Cytrans®, composed of carbonate apatite (CO_3Ap) [27,28].

2. Materials and methods

2.1. Bone graft materials

mRCP (FUJIFILM, Tokyo, Japan) from human type I collagen α chain was prepared as previously described [17,29–32]. Briefly, a 10 wt % RCP solution was gelled and freeze-dried to form porous sponge blocks which were crushed into particles and cross-linked via a heat-dependent dehydration condensation reaction for 4.75 h. The mRCP particles had an average diameter of 1000 μm [20]. Cytrans® granules, herein referred to as CA, were purchased from GC Corporation (Tokyo, Japan) and had an average diameter of 1356 μm.

2.2. Animals

Nine-week-old healthy male Sprague-Dawley rats with body weights of 260–300 g were used in this study (Japan SLC, Inc.

Nagoya, Japan). The rats were housed in an animal experimentation laboratory and fed a standard diet at the Animal Research Center of the Aichi Gakuin University. The study protocol was approved by the Animal Care and Use Committee of the School of Dentistry, Aichi Gakuin University (Approval No. AGUD412). All animal handling and surgical procedures were performed in accordance with the Regulations on Animal Experimentation of the School of Dentistry, Aichi Gakuin University.

2.3. Surgical procedure

The rats were anesthetized by inhalation of 3.0% isoflurane (Mylan, Canonsburg, Pennsylvania, USA) in 70% nitrous oxide and 30% oxygen with a face mask. The dorsal portion of the head was shaved and disinfected with povidone-iodine solution. To achieve local anesthesia, 2% lidocaine (AstraZeneca, Osaka, Japan) was administered to the calvarial subcutaneous tissue, and an incision was made into the calvarial skin, followed by a square incision on the periosteum, and then a periosteal flap was elevated to expose the calvarial bone. A critical-size bone defect with a diameter of 5 mm was created using a 5.0 mm trephine bur (Meisinger, Neuss, Germany) operating at 1500 rpm or less under continuous saline irrigation of the exposed bone. The defect was filled with either 3 mg mRCP (mRCP group, n = 5) (Fig. 1A–C), 18 mg CA (CA group, n = 5) (Fig. 1D–F), or left untreated (control group, n = 5). After implantation, the periosteal flap was repositioned and the wounds were closed using 4–0 Vicryl sutures (Ethicon Inc., GA, USA).

2.4. Micro-computed tomography (μ-CT) analysis of bone regeneration

To evaluate the volume and bone mineral density (BMD) of newly formed bone in each group and the neighboring calvaria *in vivo* X-ray μ-CT (Cosmo Scan GX; Rigaku Corporation, Tokyo, Japan) was used for imaging analysis as described previously [18,20,22,33,34]. Briefly, the exposure parameters were 18 s, 90 kV, and 100 μA and the isotropic voxel size was 45 μm. μ-CT images were obtained on the day of surgery and 4, 8, and 12 weeks after surgery. Bone volume was measured in the regions of interest (ROIs) from voxel images using the 3 by 4 viewer 2019 software (Kitasenjyu Radist Dental Clinic i-View Image Center, Tokyo, Japan). The ROI size was 2.5 mm (radius) × 2.5 mm (radius) × 3.14 × 0.8 mm (depth) which covered the entire defect area. The software compared the ROIs from week 0 (immediately after surgery) to the ROIs from 4, 8 and 12 weeks after surgery and obtained values corresponding to new bone, native calvarial bone and the new bone/native calvarial bone overlapping area. Bone volume was calculated by the addition of the values corresponding to the new bone and the new bone/native calvarial bone overlapping area.

In addition, since CA granules have a CO_3Ap composition [27], the CA granules resembled natural calvarial bone in the μ-CT images, thus for the CA group, we also measured the bone volume including the CA granules. This was defined as the total bone volume, and was calculated as the sum of the values corresponding to the new bone, natural calvarial bone, and new bone/natural calvarial bone overlapping region.

BMD was calculated by comparing the measurements to a calibration curve of the bone mineral content obtained by scanning a hydroxyapatite phantom (No.0802-08, RATOC, Tokyo, 13 Japan) using the 3 by 4 viewer 2019 software.

2.5. Histological analysis

The rats were euthanized in a carbon dioxide bath 4, 8, and 12 weeks after surgery. The implant site and surrounding tissues were harvested and fixed in 4% neutral buffered paraformaldehyde for 24 h at 4 °C. Tissue specimens were decalcified in 10% ethylenediaminetetraacetic acid disodium salt (Muto Pure Chemicals, Tokyo, Japan) for 8 weeks, dehydrated through a graded series of ethanol solutions, and embedded in paraffin. Subsequently, 5 μm thick coronal plane sections were prepared with a microtome (Leica RM2165; Leica Microsystems, Nussloch, Germany) and stained with hematoxylin and eosin (H&E) (Septsapie, Tokyo, Japan) to evaluate bone formation areas and their integration into the neighboring native calvarial bone under optical microscopy. To confirm the presence of osteoclasts at the defect site, sections were

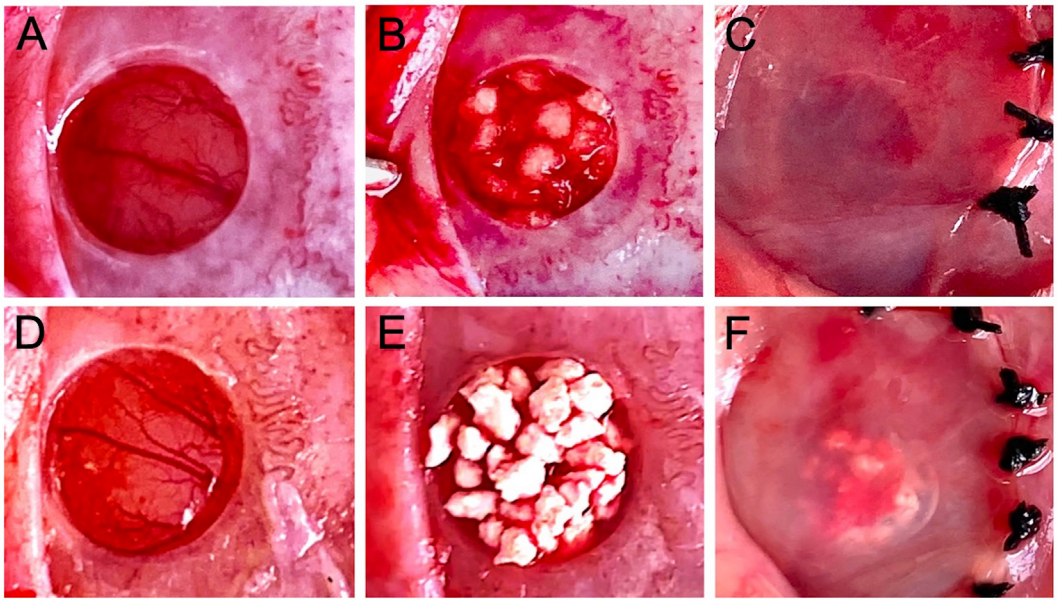

Fig. 1. Macroscopic appearance of the critical-size calvarial bone defect before and after implantation with bone graft materials. (A and D) 5 mm diameter critical size defects made with a trephine bur. The defects were filled with 3 mg mRCP (B) or 18 mg CA (E). Defects after the periosteal flap were repositioned and sutured in the (C) mRCP and (F) CA groups.

stained using a tartrate-resistant acid phosphatase (TRAP) staining kit (294-67001, Wako, Japan) following the manufacturer's instructions. TRAP-positive cells with more than 2 nuclei were counted as osteoclasts. Osteoblasts were detected using an alkaline phosphatase (ALP) staining kit (294-67001, Wako, Japan), and the ALP-positive area based on the entire area of the defect was calculated using the image analysis software ImageJ (National Institutes of Health, Bethesda, MD, United States).

2.6. Histomorphometric analysis

Histomorphometric analysis of the newly formed bone area within the bone defect (5.0 mm × 0.8 mm) of each group was performed using the ImageJ software. Briefly, for each time point (4, 8, and 12 weeks after surgery), three specimens per group were analyzed to measure the following: bone area in the entire defect area, newly formed bone at different locations in the defect site, bone union level (based on new bone bridging between the newly formed bone and host bone), and amount of residual implanted material. The level of newly formed bone was calculated based on the defect width and the bone fill measurements in the peripheral area (1.25 mm × 0.8 mm) on both sides (1.25 mm × 0.8 mm × 2) and the central area (2.5 mm × 0.8 mm) (Fig. 2A). The level of bone union was calculated based on the defect width and the bone fill measurements on the top side (periosteal side, 5.0 mm × 0.4 mm) and the bottom side (dura mater, 5.0 mm × 0.4 mm) (Fig. 2B).

Additionally, as was done with the total bone volume measurement, for the CA group, an additional measurement was performed in which the CA granules were included. This was defined as the total newly formed bone area in the entire defect.

To compare the resorption rate between the two bone graft materials, the amount of residual mRCP and CA at 12 weeks after implantation was measured and analyzed using ImageJ software.

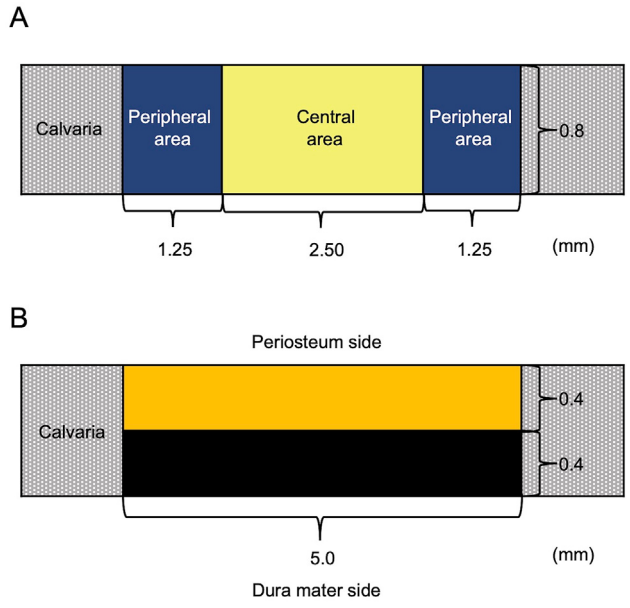

Fig. 2. Diagram of the critical-size bone defect in rat calvaria and histomorphometric analyses. (A) The amount of newly formed bone was calculated based on the defect width and the bone fill measurements in the peripheral area (1.25 mm × 0.8 mm) of both the sides (1.25 mm × 0.8 mm × 2) and the central area (2.5 mm × 0.8 mm). (B) The level of newly formed bone was calculated based on the defect width and the bone fill measurements on the top side (periosteum side, 5.0 mm × 0.4 mm) and the bottom side (dura mater side, 5.0 mm × 0.4 mm).

2.7. Statistical analyses

Data are expressed as mean ± standard deviation (SD) for each group. Statistical analysis was performed using the GraphPad Prism 9 software (GraphPad Inc., La Jolla, CA, USA). One-way analysis of variance (ANOVA) with Tukey's multiple comparison test was used for intergroup comparisons. P was set at < 0.05.

3. Results

3.1. μ-CT analysis of hard tissue formation in the critical-size defects

To visualize and quantify the degree of hard tissue formation in the implant groups, μ-CT analysis was performed at 0, 4, 8, and 12 weeks after surgery (Fig. 3). Two-dimensional images in the coronal plane, as well as 3D reconstructed μ-CT images in the axial plane of the implant site were obtained. The mRCP group showed that 4 weeks after surgery, bone formation had taken place based on the radiopacity and considerable bone bridging seen in the defect area, with an increase in radiopacity intensity and bone bridging at 8 weeks, showing a continuous radiopaque area that covered the entire defect at 12 weeks after surgery and the radiopacity was comparable to that of the adjacent natural bone, this increase in size was also confirmed in the corresponding 3D reconstructed μ-CT images (Fig. 3A). In the CA group, from the day of surgery, the defect site exhibited a radiopaque area corresponding to the CA granules that appeared arranged as a compact network. At 4 weeks after surgery, the size of the radiopaque area around the edges of the defect increased, and was displayed as a small amount of new bone that filled the space between the granules in the 3D reconstructed μ-CT images. While at 12 weeks after surgery, this radiopaque area showed a more uniform appearance between the granules and slight increase in the size of the new bone (Fig. 3B). No new bone formation was apparent in the samples from the control group, even after 12 weeks of surgery, with only a slight increase in the radiopaque area bordering the defect edges, these findings were consistent with the 3D reconstructed μ-CT images (Fig. 3C). To quantify the change in the bone volume at the defect site over time, the specialized 3 by 4 viewer 2019 software (Kitasenju Radist Dental Clinic i-View Image Center, Tokyo, Japan) was used. The data showed that the bone volume in the mRCP group increased, showing a significant difference at 8 and 12 weeks compared to that at 4 weeks after surgery (Fig. 3D). The amount of bone volume in the mRCP group was significantly higher than that of the CA and control groups at 4, 8, and 12 weeks after surgery. In the CA group, there was a significant difference in the increase in bone volume between 4 and 12 weeks after surgery. The bone volume in the CA group was significantly greater than that in the control group at 4, 8, and 12 weeks after surgery. In the control group, a significant increase in bone volume was detected at 12 weeks after surgery compared to 4 and 8 weeks after surgery (Fig. 3D). The total bone volume in the CA group was greater than that of the control and mRCP groups at 4 weeks after surgery. However, the total bone volume in the CA group did not change significantly during the study period. Noticeably, at 12 weeks after surgery, the total bone volume in the CA group and the mRCP group was comparable (Fig. 3E).

We next measured the BMD in the mRCP and CA groups at 4, 8, and 12 weeks after surgery and compared it to the BMD of the native calvarial bone. Our results showed that the mRCP group had a significantly lower BMD than the native calvarial bone after 4 and 8 weeks, although at 12 weeks, the BMD in the mRCP group was comparable to that of the native calvarial bone. However, there was no significant difference in BMD between the CA group and the native calvarial bone group at any time point after surgery (Table 1).

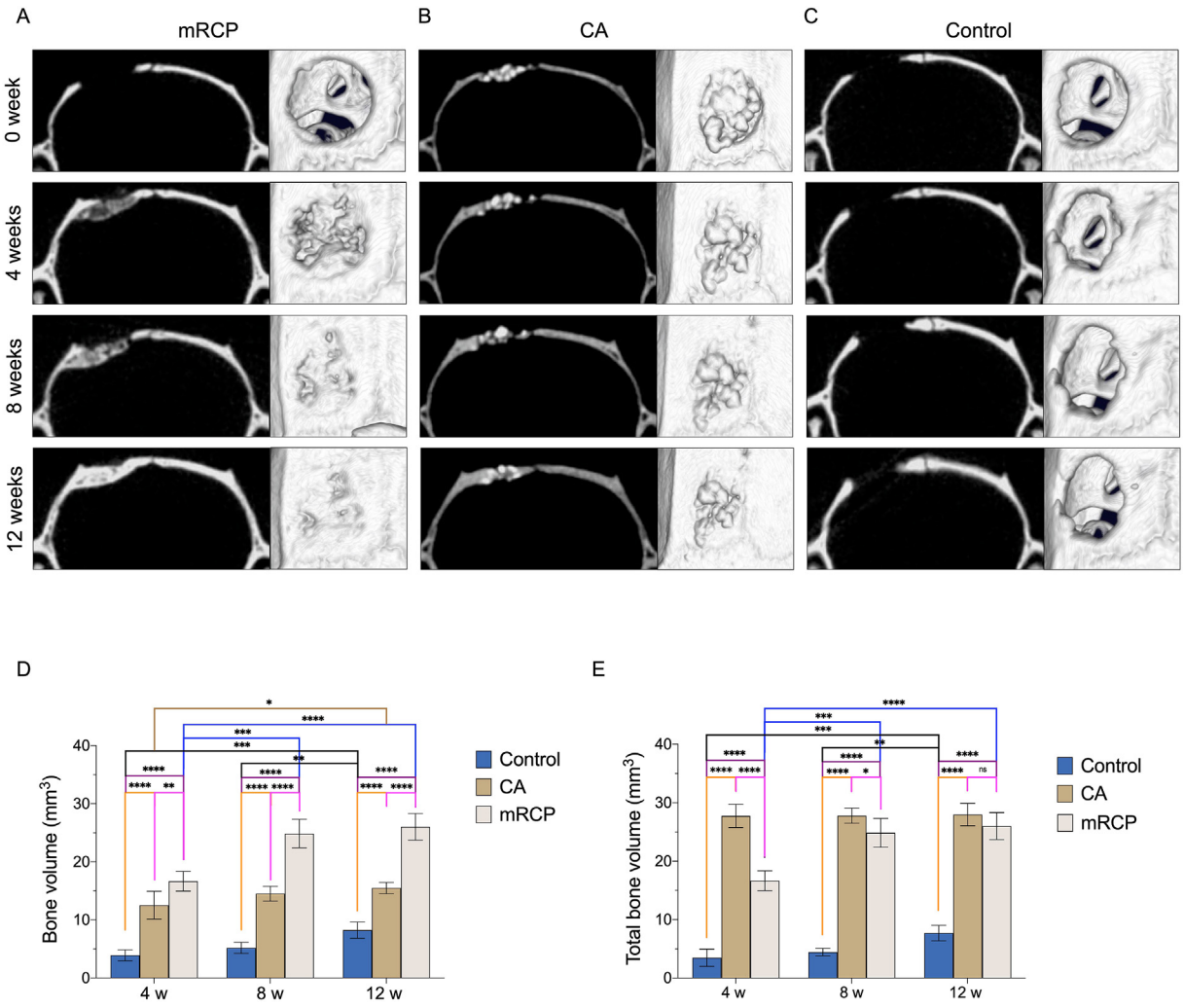

Fig. 3. Representative coronal and axial plane images of μ-CT and 3D reconstructed μ-CT analysis of the calvarial bone defects in the (A) mRCP (B) CA and (C) control groups at 0, 4, 8, and 12 weeks after implantation. Amount of bone volume (D) and total bone volume (E) in the calvarial bone defects at 4, 8, and 12 weeks after implantation with bone graft materials assessed by μ-CT. *P < 0.05, **P < 0.01, ***P < 0.001, and ****P < 0.0001. The columns and error bars in the graphs represent the mean and standard deviation (SD), respectively (n = 5 per group).

3.2. Histological analysis of newly formed bone

We continued our assessment of the newly formed bone using H&E staining, which allowed us to distinguish the newly formed bone from grafted materials and their integration into the host tissue. In our previous studies [20,22], H&E staining showed that newly formed bone was characterized by pink-stained structures, and the remnant mRCP particles were stained violet. Low- and high-magnification images of the mRCP group revealed that newly formed bone was apparent at 4 weeks after implantation, as shown by the abundant bony tissue islands in the network of remnant mRCP stained in violet. Although the boundary with the peripheral bone could be distinguished, some newly formed bone fragments had fused with peripheral bone (Fig. 4A). At 8 weeks, the regenerated bone fragments were larger and began to resemble lamellar structures that contained vessels and osteocyte-like cells, with a decrease in the remnant mRCP surrounding the bone fragments (Fig. 4B). At 12 weeks, the newly formed bone structures had grown considerably and were more evident in the periphery and bottom sides of the defect, with the borderline between the native and regenerated bone almost indistinguishable. A substantial amount of resorption of the mRCP particles was also observed (Fig. 4C). In

Table 1
Bone mineral density (BMD) in the implant site assessed by μ-CT analyses. The BMD was measured in the mRCP group, CA group, and compared with the neighboring native calvaria bone (n = 5) at 4, 8, and 12 weeks after implantation. *P < 0.05, ****P < 0.0001.

BMD (mg/cm^3)			
Group	4 weeks	8 weeks	12 weeks
mRCP (n = 5)	474 ± 7****	542 ± 8*	588 ± 1
CA (n = 5)	558 ± 2	543 ± 2	550 ± 2
Native calvarial bone (n = 5)	568 ± 8	572 ± 1	579 ± 9

BMD: bone mineral density, mRCP: medium-cross-linked recombinant collagen peptide, CA: carbonate apatite.

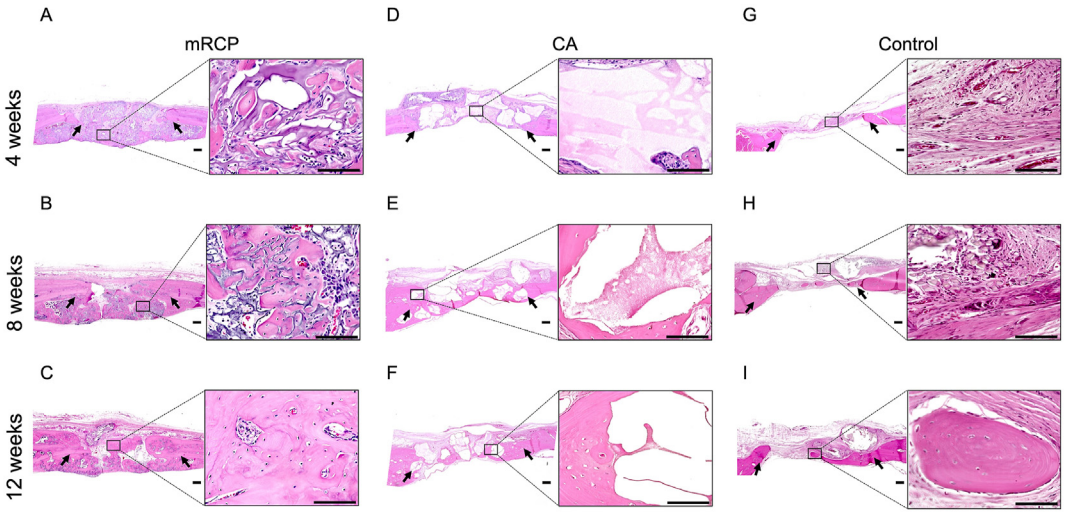

Fig. 4. Representative histological images at low (× 20) and high (× 400) magnification (enlarged view of boxed area) of H&E-stained sections of the critical-sized bone defects of the (A–C) mRCP, (D–F) CA, and (G–I) control groups at 4, 8, and 12 weeks after surgery. Scale bars represent 300 μm and 100 μm in the enlarged boxed area. The arrows indicate the boundary between the implanted site and the native calvaria bone. The pink-stained structures in the defect indicate newly formed bone. Scale bars represent 300 μm and 100 μm (enlarged boxed area).

the CA group, the CA particles were seen as light pink or white spaces in the H&E images. Four weeks after implantation, the CA group showed large particles surrounded by fibrous connective tissue (Fig. 4D). By 8 weeks, pink-stained structures had formed around the CA fragments, which appeared to show some signs of degradation, as noted by the resorption cavities in the border of the CA fragments (Fig. 4E). Twelve weeks after transplantation, the pink-stained newly formed bone grew considerably to form lamellar structures that appeared to have replaced some of the CA particles that had been resorbed, being more prominent on the bottom side of the defect (Fig. 4F). In the control group, only a small amount of new bone formation was observed towards the end of the study period (Fig. 4G–I).

3.3. Histomorphometric analysis of the critical-size defects

To accurately assess the process of bone formation, we used H&E-stained sections to measure the amount of newly formed bone at the following sites: the entire defect, the peripheral sides (left and right) compared to the central side of the defect, and the top (periosteal side) compared to the bottom (dura mater side) of the defect, as previously described [20,22]. Our previous report showed the bone forming potential of mRCP at 4 weeks after surgery [20]. In this study, we observed that there was a significantly greater amount of newly formed bone at 8 and 12 weeks than at 4 weeks after implantation (Fig. 5A). The amount of newly formed bone in the mRCP group was significantly greater than that in the CA and control groups at every time point. Although the amount of newly formed bone in the CA group significantly increased over time, it was only significantly greater to that of the control group at 4 weeks after surgery (Fig. 5A).

In contrast, when measuring the amount of total newly formed bone in the entire defect, it was found that the amount of total newly formed bone in the CA group was significantly greater than that of the mRCP and control groups at 4 and 8 weeks after surgery. However, at 12 weeks after surgery, the amount of total newly formed bone in the CA group was comparable to that of the mRCP group (Fig. 5B).

When comparing the newly formed bone between the peripheral sides and the center of the defect site, mRCP showed a greater amount of bone formation in the periphery of the defect at all time points observed (Fig. 6A). In the CA group, there was no significant difference in the amount of newly formed bone between the central and peripheral areas at 4, 8, and 12 weeks after surgery (Fig. 6B). The bone formed at the bottom side (dura mater) of the defect was significantly larger than that at the top side (periosteal side) in the

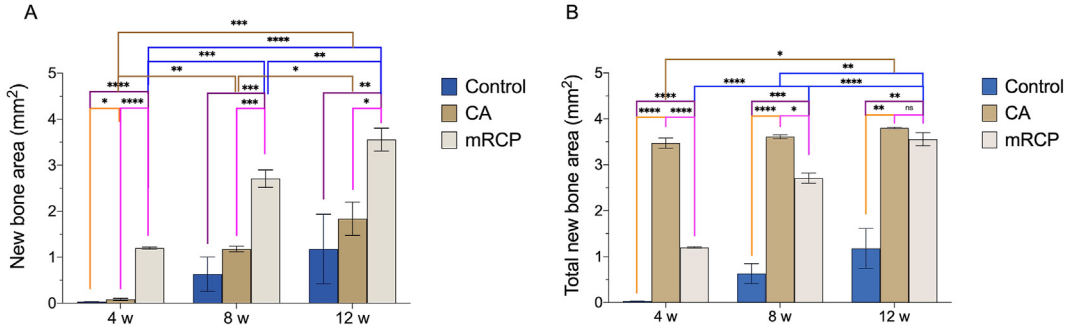

Fig. 5. Histomorphometric analysis of the newly formed bone area (A) and total newly formed bone area (B) in the entire bone defect in the mRCP, CA, and control groups at 4, 8, and 12 weeks after implantation. Newly formed bone and total newly formed bone areas in the entire defect (5.0 mm × 0.8 mm) were measured using ImageJ. *P < 0.05, **P < 0.01, ***P < 0.001 and ****P < 0.0001. The columns and error bars in the graph represent the mean and SD (n = 3), respectively. ns: not significant.

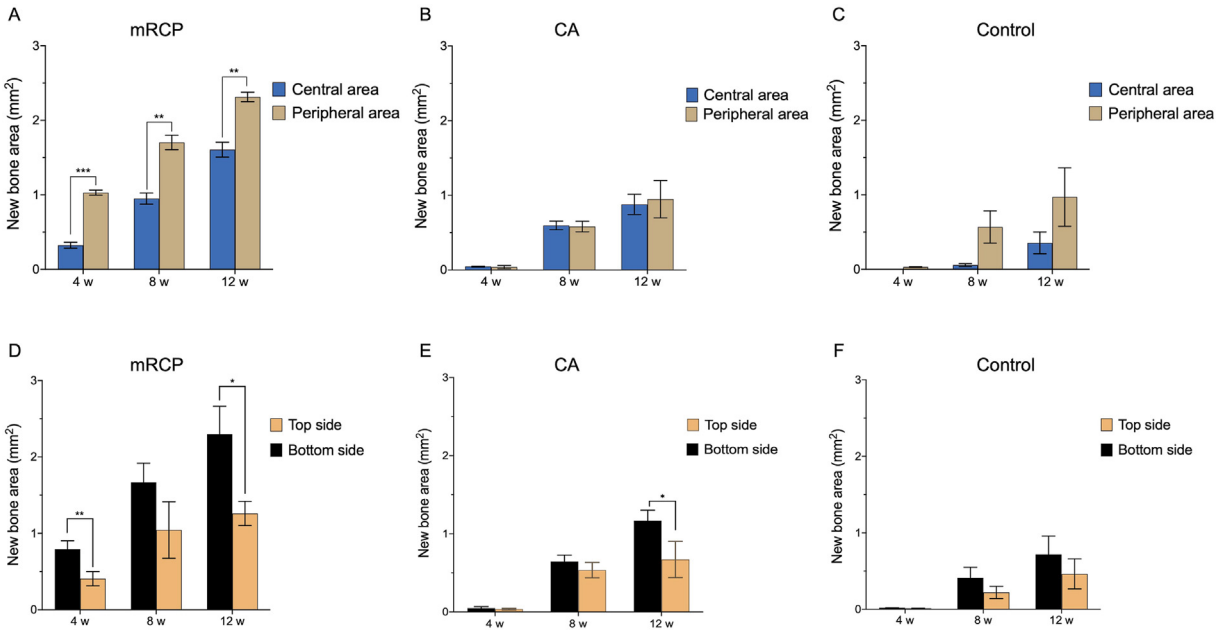

Fig. 6. Newly formed bone areas at different locations in the defect site of the implanted groups at 4, 8 and 12 weeks after surgery. The newly formed bone in the peripheral areas on both sides (1.25 mm × 0.8 mm × 1.25 mm) were compared with the central area (5.0 mm × 0.8 mm) of the bone defect in the (A) mRCP, (B) CA, and (C) control groups. Newly formed bone in the top side (5.0 mm × 0.4 mm) and the bottom side (5.0 mm × 0.4 mm) of the entire bone defect in the mRCP (D), CA (E), and (F) control groups. The newly formed bone areas were measured using ImageJ. *P < 0.05, **P < 0.01, and ***P < 0.001. The columns and error bars in the graph represent the mean and SD (n = 3), respectively.

mRCP group at 4 and 12 weeks after implantation and after 12 weeks in the CA group (Fig. 6D and E). The control group did not show significant differences in the amount of bone formation at defect sites throughout the experimental period (Fig. 6C and F).

A direct comparison of the newly formed bone at different sites of the defect among the groups showed that the mRCP group had significantly more newly formed bone at the central area compared to that of the CA and control groups at every observed time point,

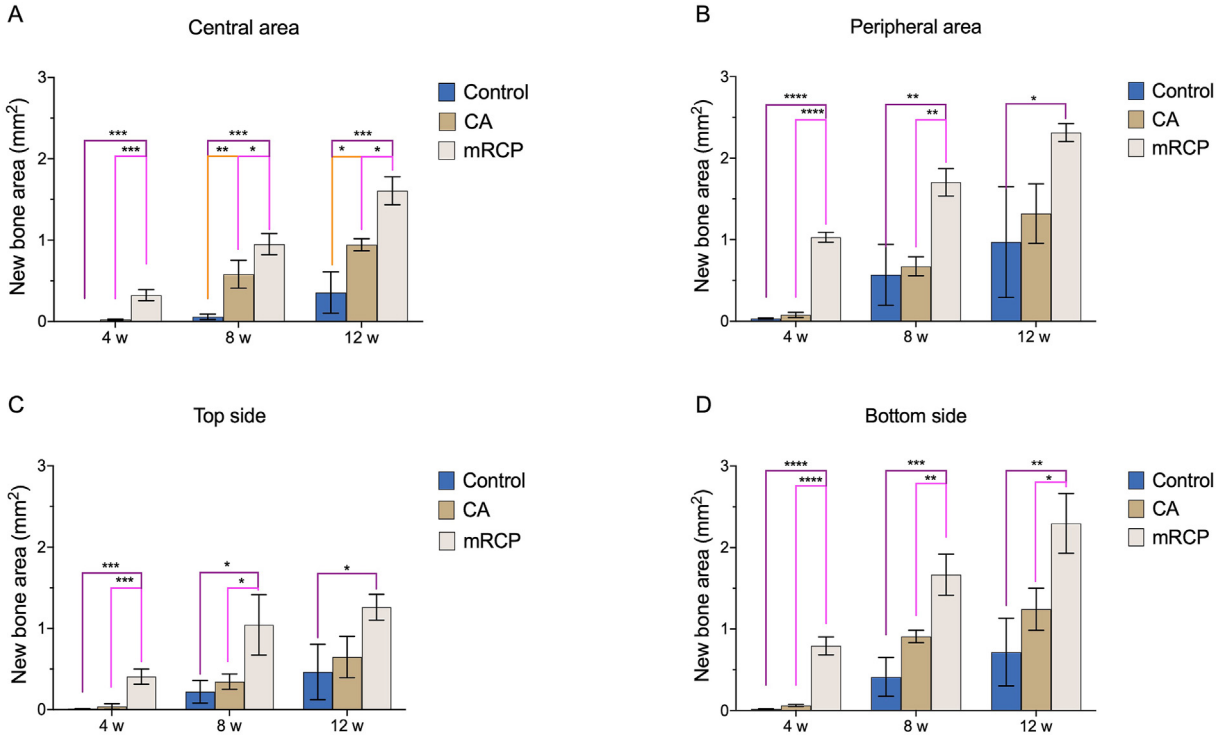

Fig. 7. Comparison of the newly formed bone areas between the three groups at different locations in the defect site at 4, 8, and 12 weeks after surgery. (A) central area (2.5 mm × 0.8 mm), (B) peripheral area on both sides (1.25 mm × 0.8 mm × 2), (C) top side (5.0 mm × 0.4 mm), and (D) bottom side (5.0 mm × 0.4 mm) of the defect were measured from the entire calvarial bone defect using ImageJ. *P < 0.05, **P < 0.01, ***P < 0.001, and ****P < 0.0001. The columns and error bars in the graph represent the mean and SD (n = 3), respectively. ns: not significant.

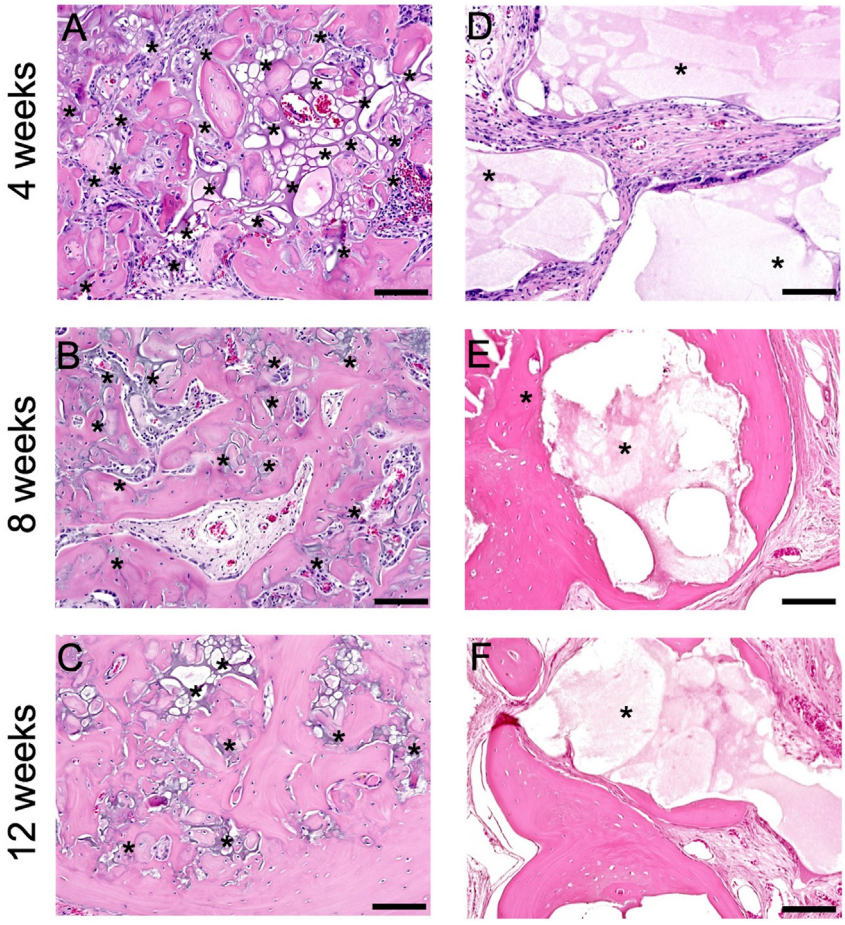
A
B
C
D
E
F
4 weeks
8 weeks
12 weeks

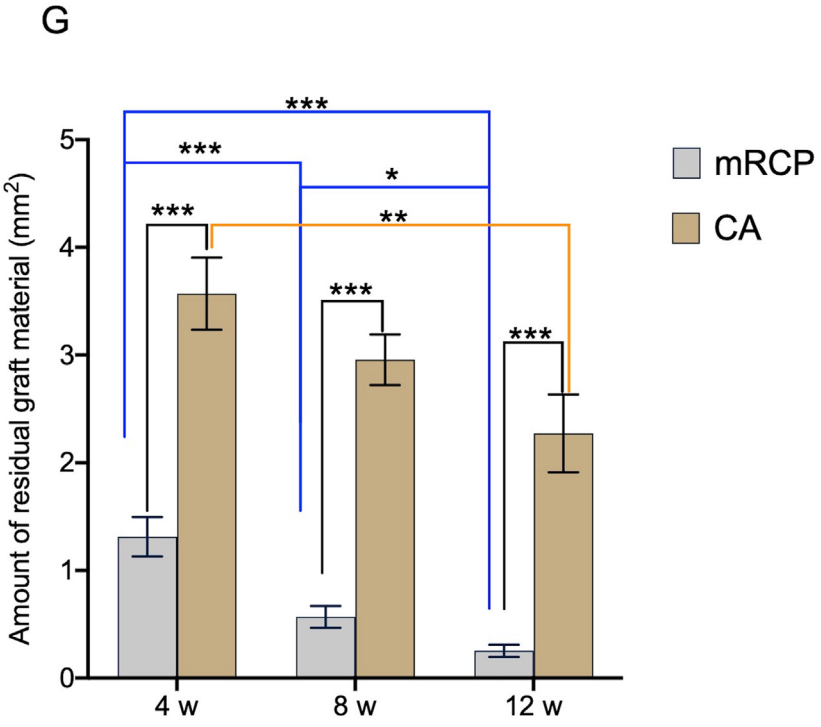
G
Amount of residual graft material (mm2)
0
1
2
3
4
5
4 w
8 w
12 w
***
***
*
***
**
***
***
mRCP
CA

while the CA group had significantly more newly formed bone compared to the control group at 8 and 12 weeks after surgery (Fig. 7A). In the peripheral area, the mRCP group had significantly more newly formed bone compared to the control group at 4, 8, and 12 weeks after surgery and to the CA group at 4 and 8 weeks after surgery (Fig. 7B). There were no significant differences in the levels of bone formation between the CA and control groups (Fig. 7B). The similar tendencies in the amount of newly formed bone between each group were observed at the top side (periosteal side) (Fig. 7C) and at the bottom side (dura mater side) of the defect (Fig. 7D).

Having observed that mRCP clearly promoted bone generation beyond four weeks, as we previously reported [20,22], we next sought to understand how its physical properties changed over this longer period of observation. Since biodegradability is a fundamental desirable feature of any bone graft material [4,35,36], we measured the amount of residual mRCP at 4, 8, and 12 weeks after implantation. As shown in Fig. 8, there was a prominent decrease in the residual mRCP over time, which was significantly decreased at 12 weeks compared to that at 4 weeks after surgery (Fig. 8A–C and G). The resorption of CA granules was modest, as shown by the appearance of irregular edges and resorption cavities in the granules compared to the straight borders at 4 weeks, although at 12 weeks, a significantly greater amount of residual material was observed compared to mRCP (Fig. 8D–F and G). This is in agreement with previous reports on CA granules and their resorption, in which the material was observed even after 24 weeks of implantation in other animal models [37].

The significant levels of newly formed bone generated by mRCP together with its significant resorption *in vivo* led us to further investigate its stimulating effect on bone remodeling by observing osteoclast and odontoblastic activity compared to that of CA and control groups. Therefore, TRAP staining was performed to confirm the presence of osteoclasts in the defect site. Osteoblasts were detected by ALP staining, and the ALP-positive area based on the entire defect area was calculated at 4, 8, and 12 weeks after implantation. In the mRCP group the number of osteoclasts was higher at 8 weeks after implantation than at 4 and 12 weeks (Fig. 9A–C and J). The number of osteoclasts in the mRCP group was significantly higher than that of the CA and control groups at 4, 8, and 12 weeks after surgery. In the CA and control groups, the number of osteoclasts did not change significantly during the study period and there was no statistical difference between both groups (Fig. 9D–I and J). ALP staining in the mRCP group showed osteoblast activity throughout the study period (Fig. 10A–C); however, no significant differences were found in the ALP-positive area between 4, 8, and 12 weeks after implantation (Fig. 10J Notably, the ALP-positive area in the mRCP group was significantly greater than that of the CA and control groups at 4 and 8 weeks after surgery (Fig. 10J). The ALP-positive area in the CA and control groups did not change significantly during the observed time points and showed no statistical difference between them (Fig. 10D–I and J).

4. Discussion

In this study, we evaluated the bone-regenerative potential of mRCP over a 12-week implantation period to validate mRCP as a suitable material for bone regeneration and to compare it with a commercially available artificial bone substitute. Our results showed that mRCP promoted bone formation through significant osteoclast activation during the late stages of healing.

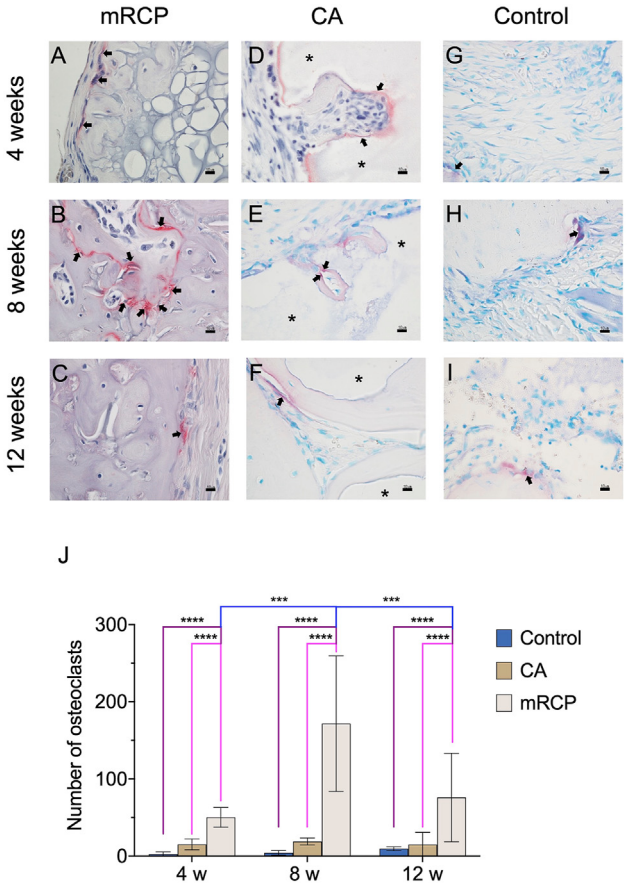

Fig. 9. Detection of osteoclasts in the critical-size bone defect of the mRCP, CA and control groups after 4, 8, and 12 weeks. High-magnification (× 600) images of tartrate-resistant acid phosphatase (TRAP)-stained sections of the (A–C) mRCP, (D–F) CA, and (G–I) control groups. Scale bars represent 10 μm. Arrows indicate osteoclasts. (J) Quantification of TRAP-positive cells at 4, 8, and 12 weeks after implantation with bone graft materials. ***P < 0.001 and ****P < 0.0001. Asterisks indicate CA granules. The columns and error bars in the graph represent the mean and SD (n = 3), respectively.

We have previously shown the bone-forming potential of mRCP after 4 weeks of implantation in a rat critical-size calvarial defect model [20,22], In this study, mRCP showed levels of bone formation 4 weeks after implantation consistent with our previous findings; however, at 12 weeks after implantation, there was a substantial increase in both the bone volume and newly formed bone as assessed by μ-CT and histological analysis, respectively.

Previous reports from our laboratory and others have documented the bone-regenerative potential of collagen-based biomaterials in rat calvarial defects. However, to the best of our knowledge, the osteogenic induction activity of mRCP has not been examined in detail. Therefore, we focused on evaluating the biodegradability and osteogenic-inducing ability of mRCP at 4-weekly intervals over an extended period. The rationale behind the longer evaluation period compared with our previous studies stems from the fact that a steady biodegradation rate of the bone graft is highly desirable [12,38–40]. This balance has been shown to offer a stable surface for bone healing and enable bone regeneration to progress continuously at later stages of the healing process [41]. In case of large bone defects that require longer healing times, such

Fig. 8. Residual mRCP (A–C) and CA (D–F) in the implanted site after 4, 8 and 12 weeks of surgery (× 200). Scale bar represents 100 μm. (G) The graph shows the means and SD (n = 3) of the amount of residual mRCP and CA after 4, 8, and 12 weeks of surgery measured by ImageJ. *P < 0.05, **P < 0.01, and ***P < 0.001. Asterisks indicate residual bone graft. The columns and error bars in the graph represent the mean and SD (n = 3), respectively.

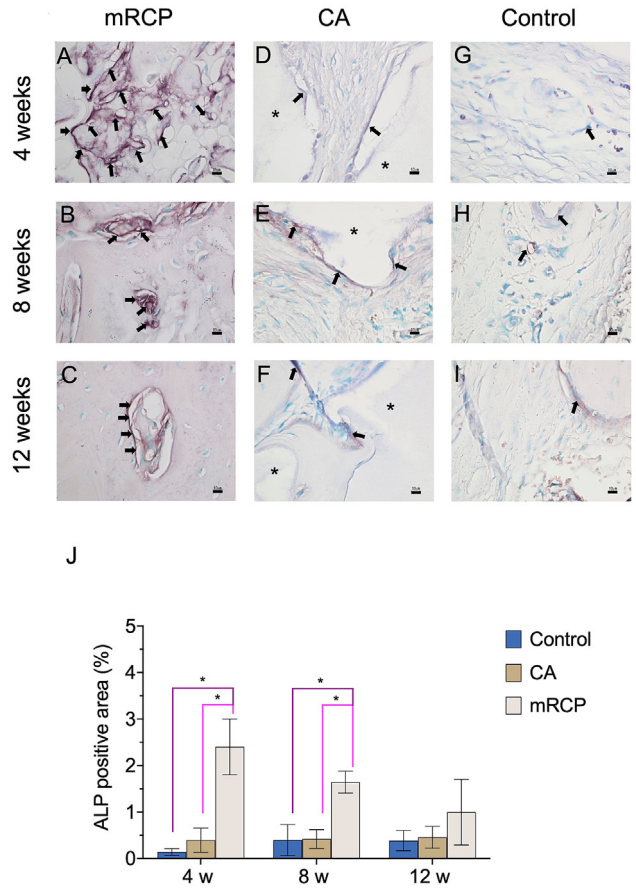

Fig. 10. Histological analysis of high-magnification (× 600) images of alkaline phosphatase (ALP)-stained sections of the critical-size bone defect in the mRCP, CA and control groups after 4, 8, and 12 weeks. ALP-stained sections in the (A–C) mRCP, (D–F) CA, and (G–I) control groups. Scale bars represent 10 μm. Arrows indicate osteoblasts. (J) The ALP positive area was calculated at 4, 8, and 12 weeks after implantation with bone graft materials using ImageJ software. *P < 0.05. Asterisks indicate CA granules. The columns and error bars in the graph represent the mean and SD (n = 3), respectively.

as alveolar clefts, the bone graft must sufficiently resist initial degradation [12]. Moreover, clinical investigations of alveolar cleft repair by bone grafts initiate orthodontic movement 12 weeks after grafting when adequate bone density is achieved, and bone graft resorption is not complete [42,43]. Eight weeks after implantation, we observed a significant reduction in the remnant mRCP as well as an increase in newly formed bone, suggesting that sufficient material remained to offer a suitable substrate for bone remodeling to take place at later stages of the evaluation period, albeit at a different rate than CA. In this study, we used medium-crosslink RCP, which may explain the resistance of RCP to degradation. This may be attributed to the heat-mediated cross-linking of the RGD chains, which optimizes biodegradation activity [12] and helps to maintain other essential properties of collagen-based biomaterials [44–49]. Therefore, this study provides useful information on the progress of biodegradation of mRCP particles at weekly intervals.

The authors considered CA as a suitable reference bone graft material due to its design oriented to dental and maxillofacial surgeries [27], usage in clinical investigations, and commercial availability [28]. Additionally, in animal models of bone defects implanted with CA for 12 weeks, CA had undergone a degree of resorption and replacement by bone but still largely remained at the implant site [27,37]. This property is attributed to the CO_3Ap composition of CA, resembling natural bone, and its remodeling rate [27], serving as a substitute for bone while promoting new bone formation. Therefore, when measuring the total bone volume and the total newly formed bone by μ-CT and histomorphometric analysis, respectively, the CA granules were included in both measurements. Although the baseline levels of the total bone volume and total newly formed bone in the CA group were high, there were no changes in these measurements during the 12-week observation period. This is likely due to the large amount of residual CA and the slow rate of new bone formation relative to mRCP.

The structure of CA may have also had a role in these findings. In this study we used a commercial version of CA granules that contains no pores, while in another study, investigators performed experiments with self-manufactured CO_3Ap granules with pores and examined bone formation in rabbit calvarial defects [50]. Although their study did not show a significant difference in the resorption of pore-containing CO_3Ap granules and commercially available CA without pores, there was a tendency for the former to show mature bone formation inside the pores, that could lead to an increase in total bone formation over time. In the future, we might need to compare the effectiveness of mRCP and CO_3Ap granules with pores for bone-forming potential.

For physiological bone remodeling to take place, osteoclasts and osteoblasts must synchronize bone resorption and formation. Osteoclasts play a pivotal role in maintaining this balance by recruiting osteoblast progenitors or by directly stimulating osteoblast formation through their secreted products. This process also occurs in the healing of bone defects, a feature that has been well-exploited in the design of collagen-based bone graft materials [51,52]. The modulation of osteoclast activity by collagen-based biomaterials occurs through interactions with osteoclast signaling molecules and receptors. Co-stimulation of the receptor activator of the nuclear factor κB/RANK ligand/osteoprotegerin axis and osteoclast-associated receptor (OSCAR) leads to osteoclast activation. Specifically, collagen I, II, and III found in the bone extracellular matrix (ECM) are ligands for OSCAR [53]. Similar to our previous investigations [11,20,22], mRCP particles elicited osteoclast activation at the implant site, as evidenced by the detection of TRAP-positive cells at 4 weeks after implantation. However, in the current study, we found a higher number of osteoclasts at 8 weeks after implantation compared to that at 4 and 12 weeks. This coincided with the time of the greatest degradation of the material and occurred several weeks before the peak of new bone formation (at 12 weeks). Therefore, this suggests that sufficient mRCP particles remained to orchestrate the differentiation of osteogenic progenitors at late stages in the observation period, which also coincided with the greatest increase in newly formed bone and that resorption of mRCP occurs before new bone formation. This is in agreement with the findings of other investigators who showed that biomaterial degradation mediated in part through osteoclasts precedes peak bone formation [54].

The significant increase in osteoclasts at 8 weeks could also be a result of the RGD motifs contained in mRCP, which are responsible in large part for cellular attachment and induction of osteogenic differentiation [11–14]. The RGD sequence can bind to a wide spectrum of adhesion receptors called integrins related to bone remodeling, including αvβ3 integrins, which are highly expressed in osteoclasts, and integrins involved in MSC differentiation into osteoblasts, such as α5β1 and α2β1. Moreover, studies have shown that the RGD motif aids in wound healing and angiogenesis, suggesting that this sequence provides the framework of cells necessary for new bone formation at defect sites [55–59]. Although we expected to find an increase in the number of osteoblasts over time, we did not detect a significant change in the ALP area at the observed time points; instead, we detected osteoblasts at all time points with a tendency to decrease at 12 weeks, although this was

not statistically significant. This suggests that osteoclast proliferation, in part, leads to osteoblast activation to form new bone at these stages of healing. The significantly lower number of osteoclasts and osteoblasts in the CA group reflect the smaller amount of newly formed bone relative to that of the mRCP group. The discrepancies in the osteogenic potential in our study may be attributed to previously described characteristics of the CA granules used, including its solid dense structure and its slower biodegradation relative to mRCP, limiting the space for subsequent osteogenesis. In fact, CA resorption is only carried out by osteoclasts, and its resorption can vary depending on the specific composition of CA [60]. For instance, the honeycomb block composition of CA had faster resorption and mature bone formation rates than hydroxyapatite and β-tricalcium phosphate [61]. Atsuta I. et al. reported that CA had lower osteoinductivity than autologous bone, and that the combination of both materials lead to an increased number of osteoclasts and osteoblasts, together with greater amount of bone formation compared to CA alone [62]. Under the current experimental conditions, the evidence showed that mRCP had greater osteoinductive potential than that of CA, indicating that mRCP is a versatile bone graft material with inherent properties to facilitate the recruitment of osteogenic cells.

To help explain the primary source of these osteogenic progenitor cells, we performed histomorphometric analysis at the implant site by dividing the defect into subsections and comparing new bone growth between these. In accordance with our recent reports [20,22], at 4 weeks after implantation, larger areas of new bone formation were observed in the periphery and bottom areas of the defect, which correspond to the diploë and dura mater regions, respectively. This was not surprising as it has been shown that the diploë provides progenitor cells and nutrients, whereas the dura mater plays a pivotal role in intramembranous calcification [63–65]. However, it should be noted that this tendency was detected over a longer period than that in previous reports. This suggests that the mRCP can recruit a steady flow of cells from the dura mater and diploë over an extended period.

Our findings also indicated that mRCP promoted greater amount of bone formation than the CA and control groups in the central, diploë, dura mater and periosteal sides of the rat calvarial defect. Alveolar bone grafting involves gingival and palatal mucoperiosteal flaps and their closure after placement of the bone graft, creating a space where the walls made from periosteum and denuded bone are in contact with the graft material [66]. Within the structure of the periosteum lies osteoblasts and osteoprogenitor cells that contribute to the bone repair process [67,68]. This source of osteogenic cells may be critical for successful bone repair in the alveolar cleft and we showed that mRCP had a greater osteogenic response than CA and controls in a timely manner, implying it has potential for human alveolar cleft repair.

In human alveolar cleft repair, 12 weeks after graft surgery, bone structure and alveolar height stabilizes, and subsequent therapy is recommended [43]. Therefore, mRCP may repair bone defects and provide enough bone structure at a time when prosthetic implant or orthodontic movement is required in the clinical setting. Added to the lack of risk of contamination with the use of mRCP, this shows the feasibility of mRCP for human alveolar cleft repair.

In conclusion, this study validated the usefulness of mRCP as a bone graft material over an extended period and showed that mRCP can induce greater *de novo* bone formation compared to the clinically approved and commercially available bone graft material CA. Furthermore, even when CA granules were included in the measurements, mRCP showed comparable levels of bone formation at the end of the healing period. This suggests that mRCP is well-suited to induce osteogenic cell differentiation in a timely manner and could be a promising therapy for the human alveolar cleft. Further work is necessary to verify the precise osteogenic signaling events elicited by mRCP particles, and whether the same osteoclast and osteoblast kinetics are observed in other defect models, such as the palatine fissure model [33].

Funding

This study was funded by FUJIFILM Coorportation.

Declaration of competing interest

This work was supported by the joint research expenses with FUJIFILM Corporation.

Taku Wakita and Takahiro Hiratsuka are employees of FUJIFILM Corporation.

Acknowledgements

We thank Sept Sapie CO., LTD (Tokyo, Japan) for the preparation of the paraffin sections, H&E, ALP, and TRAP staining.

References

[1] Bajaj AK, Wongworawat AA, Punjabi A. Management of alveolar clefts. J Craniofac Surg 2003;14. https://doi.org/10.1097/00001665-200311000-00005.
[2] Kyung H, Kang N. Management of alveolar cleft. Arch Craniofac Surg 2015;16. https://doi.org/10.7181/acfs.2015.16.2.49.
[3] Janicki P, Schmidmaier G. What should be the characteristics of the ideal bone graft substitute? Combining scaffolds with growth factors and/or stem cells. Injury 2011;42. https://doi.org/10.1016/j.injury.2011.06.014.
[4] Kang NH. Current methods for the treatment of Alveolar cleft. Arch Plast Surg 2017;44. https://doi.org/10.5999/aps.2017.44.3.188.
[5] Dissaux C, Ruffenach L, Bruant-Rodier C, George D, Bodin F, Rémond Y. Cleft alveolar bone graft materials: literature review. Cleft Palate-Craniofacial J 2022;59. https://doi.org/10.1177/10556656211007692.
[6] Balaji S. Alveolar cleft defect closure with iliac bone graft, rhBMP-2 and rhBMP-2 with zygoma shavings: comparative study. Ann Maxillofac Surg 2011;1. https://doi.org/10.4103/2231-0746.83144.
[7] Antoine EE, Vlachos PP, Rylander MN. Review of collagen i hydrogels for bioengineered tissue microenvironments: characterization of mechanics, structure, and transport. Tissue Eng Part B 2014;20. https://doi.org/10.1089/ten.teb.2014.0086.
[8] Li Y, Liu Y, Li R, Bai H, Zhu Z, Zhu L, et al. Collagen-based biomaterials for bone tissue engineering. Mater Des 2021:210. https://doi.org/10.1016/j.matdes.2021.110049.
[9] Gehrke SA, Aramburú Júnior J, Treichel TLE, Rodriguez F, N de Aza P, Dedavid BA. Comparative evaluation of two collagen-based biomaterials with different compositions used for bone graft: an experimental animal study. J Appl Biomater Funct Mater 2022;20. https://doi.org/10.1177/22808000221119650.
[10] Binlateh T, Thammanichanon P, Rittipakorn P, Thinsathid N, Jitprasertwong P. Collagen-based biomaterials in periodontal regeneration: current applications and future perspectives of plant-based collagen. Biomimetics 2022;7. https://doi.org/10.3390/biomimetics7020034.
[11] Ito M, Toriumi T, Hiratsuka T, Imura H, Akiyama Y, Chimedtseren I, et al. A novel bone substitute based on recombinant type i collagen for reconstruction of alveolar cleft. Materials 2021;14. https://doi.org/10.3390/ma14092306.
[12] Hiratsuka T, Ogura I, Okamura A, Fushimi H, Yamaguchi K, Nishimura I. Bioresorbable bone graft composed of an RGD-enriched recombinant human collagen polypeptide induced neovascularization and regeneration of mature bone tissue. ACS Appl Bio Mater 2020;3. https://doi.org/10.1021/acsabm.0c00986.
[13] Furihata T, Miyaji H, Nishida E, Kato A, Miyata S, Shitomi K, et al. Bone forming ability of recombinant human collagen peptide granules applied with β-tricalcium phosphate fine particles. J Biomed Mater Res B Appl Biomater 2020;108. https://doi.org/10.1002/jbm.b.34632.
[14] Nakamura K, Tabata Y. A new fluorescent imaging of renal inflammation with RCP. J Contr Release 2010;148. https://doi.org/10.1016/j.jconrel.2010.09.005.
[15] De Long WG, Einhorn TA, Koval K, McKee M, Smith W, Sanders R, et al. Bone grafts and bone graft substitutes in orthopaedic trauma surgery. The Journal of Bone and Joint Surgery-American 2007;89:649–58. https://doi.org/10.2106/00004623-200703000-00026.
[16] Fushimi H, Hiratsuka T, Okamura A, Ono Y, Ogura I, Nishimura I. Recombinant collagen polypeptide as a versatile bone graft biomaterial. Commun Mater 2020;1. https://doi.org/10.1038/s43246-020-00089-9.

[17] Nakamura K, Iwazawa R, Yoshioka Y. Introduction to a new cell transplantation platform via recombinant peptide petaloid pieces and its application to islet transplantation with mesenchymal stem cells. Transpl Int 2016;29:1039–50. https://doi.org/10.1111/tri.12810.
[18] Tateno A, Asano M, Akita D, Toriumi T, Tsurumachi-Iwasaki N, Kazama T, et al. Transplantation of dedifferentiated fat cells combined with a biodegradable type i collagen-recombinant peptide scaffold for critical-size bone defects in rats. J Oral Sci 2019;61:534–8. https://doi.org/10.2334/josnusd.18-0458.
[19] Knott L, Bailey AJ. Collagen cross-links in mineralizing tissues: a review of their chemistry, function, and clinical relevance. Bone 1998;22. https://doi.org/10.1016/S8756-3282(97)00279-2.
[20] Akiyama Y, Ito M, Toriumi T, Hiratsuka T, Arai Y, Tanaka S, et al. Bone formation potential of collagen type I-based recombinant peptide particles in rat calvaria defects. Regen Ther 2021;16. https://doi.org/10.1016/j.reth.2020.12.001.
[21] Zhang Q, Lu H, Kawazoe N, Chen G. Pore size effect of collagen scaffolds on cartilage regeneration. Acta Biomater 2014;10. https://doi.org/10.1016/j.actbio.2013.12.042.
[22] Yamahara S, Montenegro Raudales JL, Akiyama Y, Ito M, Chimedtseren I, Arai Y, et al. Appropriate pore size for bone formation potential of porous collagen type I-based recombinant peptide. Regen Ther 2022;21:294–306. https://doi.org/10.1016/j.reth.2022.08.001.
[23] Matsuoka K, Park KA, Ito M, Ikeda K, Takeshita S. Osteoclast-derived complement component 3a stimulates osteoblast differentiation. J Bone Miner Res 2014;29. https://doi.org/10.1002/jbmr.2187.
[24] Polo-Corrales L, Latorre-Esteves M, Ramirez-Vick JE. Scaffold design for bone regeneration. J Nanosci Nanotechnol 2014;14. https://doi.org/10.1166/jnn.2014.9127.
[25] Bergland O, Semb G, Aabyholm FE. Elimination of the residual alveolar cleft by secondary bone grafting and subsequent orthodontic treatment. Cleft Palate J 1986;23. https://doi.org/10.1016/0889-5406(88)90203-x.
[26] Uzel A. Orthodontics in relation with alveolar bone grafting in CLP patients. Current Approaches in Orthodontics 2019. https://doi.org/10.5772/intechopen.80853.
[27] Ishikawa K. Carbonate apatite bone replacement: learn from the bone. J Ceram Soc Jpn 2019;127. https://doi.org/10.2109/jcersj2.19042.
[28] Kitamura M, Yamashita M, Miki K, Ikegami K, Takedachi M, Kashiwagi Y, et al. An exploratory clinical trial to evaluate the safety and efficacy of combination therapy of REGROTH® and Cytrans® granules for severe periodontitis with intrabony defects. Regen Ther 2022;21:104–13. https://doi.org/10.1016/j.reth.2022.06.001.
[29] Pawelec KM, Confalonieri D, Ehlicke F, van Boxtel HA, Walles H, Kluijtmans SGJM. Osteogenesis and mineralization of mesenchymal stem cells in collagen type I-based recombinant peptide scaffolds. J Biomed Mater Res 2017;105:1856–66. https://doi.org/10.1002/jbm.a.36049.
[30] Parvizi M, Plantinga JA, Van Speuwel-Goossens CAFM, Van Dongen EMWM, Kluijtmans SGJM, Harmsen MC. Development of recombinant collagen-peptide-based vehicles for delivery of adipose-derived stromal cells. J Biomed Mater Res 2016;104:503–16. https://doi.org/10.1002/jbm.a.35588.
[31] Miyamoto M, Nakamura K, Shichinohe H, Yamauchi T, Ito M, Saito H, et al. Human recombinant peptide sponge enables novel, less invasive cell therapy for ischemic stroke. Stem Cell Int 2018;2018. https://doi.org/10.1155/2018/4829534.
[32] Suzuki D, Akita D, Tsurumachi N, Kano K, Yamanaka K, Kaneko T, et al. Transplantation of mature adipocyte-derived dedifferentiated fat cells into three-wall defects in the rat periodontium induces tissue regeneration. J Oral Sci 2017;59. https://doi.org/10.2334/josnusd.16-0878.
[33] Ito M, Toriumi T, Imura H, Akiyama Y, Arai Y, Natsume N, et al. Rat palatine fissure: a suitable experimental model for evaluating bone regeneration. Tissue Eng C Methods 2019;25. https://doi.org/10.1089/ten.tec.2019.0143.
[34] Akita D, Kano K, Saito-Tamura Y, Mashimo T, Sato-Shionome M, Tsurumachi N, et al. Use of rat mature adipocyte-derived dedifferentiated fat cells as a cell source for periodontal tissue regeneration. Front Physiol 2016;7. https://doi.org/10.3389/fphys.2016.00050.
[35] Li Y, Chen SK, Li L, Qin L, Wang XL, Lai YX. Bone defect animal models for testing efficacy of bone substitute biomaterials. J Orthop Translat 2015;3. https://doi.org/10.1016/j.jot.2015.05.002.
[36] Chatzipetros E, Damaskos S, Tosios KI, Christopoulos P, Donta C, Kalogirou E-M, et al. The effect of nano-hydroxyapatite/chitosan scaffolds on rat calvarial defects for bone regeneration. Int. J. Implant Dent. 2021;7. https://doi.org/10.1186/s40729-021-00327-w.
[37] Kanazawa M, Tsuru K, Fukuda N, Sakemi Y, Nakashima Y, Ishikawa K. Evaluation of carbonate apatite blocks fabricated from dicalcium phosphate dihydrate blocks for reconstruction of rabbit femoral and tibial defects. J Mater Sci Mater Med 2017;28. https://doi.org/10.1007/s10856-017-5896-5.
[38] Schilling AF, Linhart W, Filke S, Gebauer M, Schinke T, Rueger JM, et al. Resorbability of bone substitute biomaterials by human osteoclasts. Biomaterials 2004;25. https://doi.org/10.1016/j.biomaterials.2003.10.079.
[39] Guo Y, Chen Z, Wen J, Jia M, Shao Z, Zhao X. A simple semi-quantitative approach studying the in vivo degradation of regenerated silk fibroin scaffolds with different pore sizes. Mater Sci Eng C 2017;79. https://doi.org/10.1016/j.msec.2017.05.008.
[40] Zhang L, Liu X, Li G, Wang P, Yang Y. Tailoring degradation rates of silk fibroin scaffolds for tissue engineering. J Biomed Mater Res 2019;107. https://doi.org/10.1002/jbm.a.36537.
[41] Dumas JE, Prieto EM, Zienkiewicz KJ, Guda T, Wenke JC, Bible J, et al. Balancing the rates of new bone formation and polymer degradation enhances healing of weight-bearing allograft/polyurethane composites in rabbit femoral defects. Tissue Eng 2014;20. https://doi.org/10.1089/ten.tea.2012.0762.
[42] Xiao WL, Zhang DZ, Chen XJ, Yuan C, Xue LF. Osteogenesis effect of guided bone regeneration combined with alveolar cleft grafting: assessment by cone beam computed tomography. Int J Oral Maxillofac Surg 2016;45. https://doi.org/10.1016/j.ijom.2016.01.013.
[43] Zhang DZ, Xiao WL, Zhou R, Xue LF, Ma L. Evaluation of bone height and bone mineral density using cone beam computed tomography after secondary bone graft in alveolar cleft. J Craniofac Surg 2015;26. https://doi.org/10.1097/SCS.0000000000001766.
[44] Enomoto-Iwamoto M, Iwamoto M, Nakashima K, Mukudai Y, Boettiger D, Pacifici M, et al. Involvement of α5β1 integrin in matrix interactions and proliferation of chondrocytes. J Bone Miner Res 1997;12. https://doi.org/10.1359/jbmr.1997.12.7.1124.
[45] Chastain SR, Kundu AK, Dhar S, Calvert JW, Putnam AJ. Adhesion of mesenchymal stem cells to polymer scaffolds occurs via distinct ECM ligands and controls their osteogenic differentiation. J Biomed Mater Res 2006;78. https://doi.org/10.1002/jbm.a.30686.
[46] Shimaya M, Muneta T, Ichinose S, Tsuji K, Sekiya I. Magnesium enhances adherence and cartilage formation of synovial mesenchymal stem cells through integrins. Osteoarthritis Cartilage 2010;18. https://doi.org/10.1016/j.joca.2010.06.005.
[47] Ruoslahti E, Pierschbacher MD. New perspectives in cell adhesion: RGD and integrins. Science 1987:238. https://doi.org/10.1126/science.2821619. 1979.
[48] Eto K, Puzon-McLaughlin W, Sheppard D, Sehara-Fujisawa A, Zhang XP, Takada Y. RGD-independent binding of integrin α9β1 to the ADAM-12 and -15 disintegrin domains mediates cell-cell interaction. J Biol Chem 2000;275. https://doi.org/10.1074/jbc.M001953200.
[49] Ruoslahti E. RGD and other recognition sequences for integrins. Annu Rev Cell Dev Biol 1996;12. https://doi.org/10.1146/annurev.cellbio.12.1.697.
[50] Akita K, Fukuda N, Kamada K, Kudoh K, Kurio N, Tsuru K, et al. Fabrication of porous carbonate apatite granules using microfiber and its histological evaluations in rabbit calvarial bone defects. J Biomed Mater Res 2020;108. https://doi.org/10.1002/jbm.a.36850.
[51] Martin TJ, Sims NA. Osteoclast-derived activity in the coupling of bone formation to resorption. Trends Mol Med 2005;11. https://doi.org/10.1016/j.molmed.2004.12.004.
[52] Omi M, Mishina Y. Roles of osteoclasts in alveolar bone remodeling. Genesis 2022;60. https://doi.org/10.1002/dvg.23490.
[53] Ren X, Zhou Q, Foulad D, Tiffany AS, Dewey MJ, Bischoff D, et al. Osteoprotegerin reduces osteoclast resorption activity without affecting osteogenesis on nanoparticulate mineralized collagen scaffolds. Sci Adv 2019;5. https://doi.org/10.1126/sciadv.aaw4991.
[54] Chazono M, Tanaka T, Komaki H, Fujii K. Bone formation and bioresorption after implantation of injectable β-tricalcium phosphate granules-hyaluronate complex in rabbit bone defects. J Biomed Mater Res 2004;70. https://doi.org/10.1002/jbm.a.30094.
[55] Choi SK, Park JK, Kim JH, Lee KM, Kim E, Jeong KS, et al. Integrin-binding elastin-like polypeptide as an in situ gelling delivery matrix enhances the therapeutic efficacy of adipose stem cells in healing full-thickness cutaneous wounds. J Contr Release 2016;237. https://doi.org/10.1016/j.jconrel.2016.07.006.
[56] Yu J, Gu Y, Du KT, Mihardja S, Sievers RE, Lee RJ. The effect of injected RGD modified alginate on angiogenesis and left ventricular function in a chronic rat infarct model. Biomaterials 2009;30. https://doi.org/10.1016/j.biomaterials.2008.09.059.
[57] Dhavalikar P, Robinson A, Lan Z, Jenkins D, Chwatko M, Salhadar K, et al. Review of integrin-targeting biomaterials in tissue engineering. Adv Healthcare Mater 2020;9. https://doi.org/10.1002/adhm.202000795.
[58] Yao CH, Yang BY, Li YCE. Remodeling effects of the combination of GGT scaffolds, percutaneous electrical stimulation, and acupuncture on large bone defects in rats. Front Bioeng Biotechnol 2022;10. https://doi.org/10.3389/fbioe.2022.832808.
[59] Helfrich MH, Nesbitt SA, Horton MA. Integrins on rat osteoclasts: characterization of two monoclonal antibodies (F4 and F11) to rat β3. J Bone Miner Res 1992;7. https://doi.org/10.1002/jbmr.5650070315.
[60] Doi Y, Shibutani T, Moriwaki Y, Kajimoto T, Iwayama Y. Sintered carbonate apatites as bioresorbable bone substitutes. J Biomed Mater Res 1998;39:19980315. https://doi.org/10.1002/(SICI)1097-4636. 39:4<603::AID-JBM15>3.0.CO;2-7.
[61] Hayashi K, Kishida R, Tsuchiya A, Ishikawa K. Honeycomb blocks composed of carbonate apatite, β-tricalcium phosphate, and hydroxyapatite for bone regeneration: effects of composition on biological responses. Mater Today Bio 2019;4. https://doi.org/10.1016/j.mtbio.2019.100031.
[62] Atsuta I, Mizokami T, Jinno Y, Ji B, Xie T, Ayukawa Y. Synergistic effect of carbonate apatite and autogenous bone on osteogenesis. Materials 2022;15. https://doi.org/10.3390/ma15228100.
[63] Kpelao E, El Kader MA, Anthony BK, Alain A, Agbeko D, Hobli A, et al. Technique of granulation tissue genesis from diploe. Mod Plast Surg 2018;8. https://doi.org/10.4236/mps.2018.82002.
[64] Hobar PC, Schreiber JS, Mc Carthy JG, Thomas PA. The role of the dura in cranial bone regeneration in the immature animal. Plast Reconstr Surg 1993;92. https://doi.org/10.1097/00006534-199309000-00003.

[65] Gosain AK, Santoro TD, Song LS, Capel CC, Sudhakar PV, Matloub HS. Osteogenesis in calvarial defects: contribution of the dura, the pericranium, and the surrounding bone in adult versus infant animals. Plast Reconstr Surg 2003;112. https://doi.org/10.1097/01.PRS.0000070728.56716.51.
[66] Chu YY, Chang FCS, Lu TC, Lee CH, Chen PKT. Surgical outcomes of secondary alveolar bone grafting and extensive gingivoperiosteoplasty performed at mixed dentition stage in unilateral complete cleft lip and palate. J Clin Med 2020;9. https://doi.org/10.3390/jcm9020576.
[67] Van PT, Vignery A, Baron R. Cellular kinetics of the bone remodeling sequence in the rat. Anat Rec 1982;202. https://doi.org/10.1002/ar.1092020403.
[68] Squier CA, Ghoneim S, Kremenak CR. Ultrastructure of the periosteum from membrane bone. J Anat 1990:171.